Role of Vasogenic Edema and Tissue Cavitation in Ischemic Evolution on Diffusion-weighted Imaging: Comparison with Multiparameter MR and Immunohistochemistry

Keigo Matsumoto, Eng H. Lo, Allen R. Pierce, Haoran Wei, Leoncio Garrido, and Neil W. Kowall

PURPOSE: To examine the mechanisms of further evolution that occurs from the early to late phase after initial changes in diffusion-weighted imaging after cerebral ischemia. **METHODS:** Sprague-Dawley rats were subjected to middle cerebral artery occlusion. Diffusion-, proton density–, T1- and T2-weighted imaging were performed on days 0, 2, and 6. Histologic examination (IgG, glial fibrillary acidic protein, and cresyl violet staining) was done after scanning. **RESULTS:** Apparent diffusion coefficients (ADCs) in the ischemic hemisphere were significantly decreased on day 0. Thereafter, ADCs increased over time and became significantly higher than the contralateral side by day 6. Changes in basal ganglia occurred more rapidly than in cortex. Proton density–, T1-, and T2-weighted scans showed maximal changes on day 2. From day 0 to day 2, there are significant correlations between changes in ADC and changes in T1-weighted signals and T2-weighted signals. Histologic exam showed early neuronal injury on day 0, intense gliotic activity and protein leakage associated with infarction and edema on day 2, and cavitation in severely infarcted areas on day 6. **CONCLUSION:** After initial reduction of ADC, the subsequent increase in ADC values on day 2 may be associated with vasogenic edema and cell lysis. Later elevations in ADC may be related to cavitation of infarcted tissue.

Index terms: Brain, edema; Brain, ischemia; Magnetic resonance, diffusion-weighted; Animal studies

AJNR Am J Neuroradiol 16:1107–1115, May 1995

Diffusion-weighted imaging allows one to assess the early stages of cerebral ischemia by detecting decreased water diffusion that may be related to cytotoxic edema caused by energy depletion (1–4). However, from the intermediate to late stage, diffusion-weighted imaging shows complex temporal profiles (5–11). The mechanisms that underly these temporal profiles remain unclear but most likely reflect the cascade of ischemic evolution after the initial insult. The process of ischemic evolution includes cell swelling (1–4, 8), blood-brain barrier damage and vasogenic edema (6, 12), disruption of cell membrane integrity (9, 10), and, finally, tissue cavitation in severely damaged areas (8, 12).

To clarify the relationship between changes in diffusion-weighted images and ischemic brain damage, we compared diffusion-weighted with conventional spin-echo magnetic resonance (MR) images from the acute to late stage after middle cerebral artery occlusion (MCAO) in rats. To confirm the pathologic condition in each stage, we performed histologic examination including immunohistochemistry. Cresyl violet staining was used to assess parenchymal injury. Anti-IgG and anti–glial fibrillary acidic protein (GFAP) immunohistochemical analyses were performed to assess blood-brain barrier disruption and glial activation (13–15). By

Received September 19, 1994; accepted after revision December 19.

This study was supported in part by a generous grant from Sterling-Winthrop Pharmaceutical Research Division. Dr Matsumoto is a recipient of travel grant from the Shimamura Foundation, Kyoto, Japan.

From the Center for Imaging and Pharmaceutical Research (K.M., E.H.L., A.R.P.) and NMR Center (H.W., L.G.), Harvard Medical School, Massachusetts General Hospital, Charlestown; Department of Neurosurgery, Kyoto Prefectural University of Medicine, Kyoto, Japan (K.M.); and Geriatric Research Institutes, VA Medical Center, Bedford, Mass (N.W.K.).

Address reprint requests to Dr Eng H. Lo, Center for Imaging and Pharmaceutical Research, Harvard Medical School, MGH-East 149, Charlestown, MA 02129.

AJNR 16:1107–1115, May 1995 0195-6108/95/1605–1107
© American Society of Neuroradiology

mapping the spatial and temporal profile of ischemic injury with these methods, we examined the mechanisms of diffusion-weighted imaging changes from the acute to late stage after MCAO, especially those related to vasogenic edema, infarction, and tissue cavitation.

Materials and Methods

Animal Model and Experimental Design

All experimental protocols followed National Institutes of Health guidelines for the care and use of laboratory animals and were approved by the subcommittee on research animal care of the hospital. Male Sprague-Dawley rats (250 to 350 g, n = 11) were anesthetized with 1.0% to 1.5% halothane mixed with 95% air and 5% oxygen under spontaneous respiration. Catheters were placed in the femoral artery for monitoring arterial pressure, pH, and gases. MCAO was performed under a surgical microscope using the subtemporal approach (16). Briefly, after incision of the skin and the temporal muscle, the zygomatic arch was removed, and the temporal skull base was drilled 1 mm anterior to the foramen ovale. The dura and arachnoid were cut using a 25-gauge needle. The middle cerebral artery was occluded using a microbipolar coagulator, and the coagulated arteries were cut and removed. Coagulation was performed all the way between 2 mm proximal to the olfactory tract and the distal portion of the middle cerebral artery to induce severe ischemia reproducibly (17).

Approximately 40 minutes after occlusion, MR scanning was started. Rats were classified into three groups. In all rats, diffusion-, proton density–, T2-, and T1-weighted imaging were performed on the first day (day 0). Diffusion-weighted images with larger gradient pulses (8.06 G/cm) were obtained at 50, 70, 90, and 130 minutes after MCAO, to map the evolution of injury during the acute phase. Diffusion-weighted images with smaller gradient pulses (3.66 G/cm) were obtained at 110 minutes after MCAO to calculate apparent diffusion coefficients (ADCs). Proton density–, T2-, and T1-weighted imaging were performed at 150, 170, and 180 minutes after MCAO, respectively. On day 2 and day 6 after MCAO, the rats were reanesthetized, and diffusion-, proton density–, T2-, and T1-weighted images were obtained. In group 1 (n = 5) and group 2 (n = 3), the rats were killed immediately after MR scanning on day 6 and day 2, respectively; in group 3 (n = 3), the rats were killed after MR scanning on day 0. All the rats were perfusion fixed for subsequent histologic examination after the final MR scanning in each group.

MR Imaging

All measurements were performed on an imager/spectrometer system (SISCO, Fremont, Calif) equipped with a 2.0-T superconducting magnet (Nalorac, Martines, Calif) (proton frequency, 84 to 142 MHz) and a set of self-shielded gradient coils (Oxford Instruments, Oxford, United Kingdom). Images were acquired using a 6-cm-inner-diameter bird cage coil. To get the images reproducible, T1-weighted midsagittal scouts were taken, and seven consecutive coronal sections were selected posterior to the rhinal fissure. Four scans were averaged for each one of the 128 phase-encoding steps. The section thickness was 2 mm with a 4-cm field of view. Diffusion-weighted spin-echo images were obtained by applying square-shaped diffusion-sensitive gradient pulses (duration, 10 milliseconds; separation, 30 milliseconds) on either side of the 180 pulse with 1800/45/4 (repetition time/echo time/excitations). For calculation of ADC, two different amplitudes of diffusion gradients, 3.66 and 8.06 (G/cm) corresponding to b values of 256 and 1239 (s/mm^2), were applied. We calculated ADC and b values using the following formulas: ADC (mm^2/s) = ln (S1/S2)/(b2 − b1) where Sx is signal intensity at b = bx; b = $g^2G^2\delta^2(\Delta - \delta/3)$ where g is the gyromagnetic ratio; G is the amplitude of the diffusion gradient pulse; δ is the duration of the diffusion gradient pulse; and Δ is the separation time between the beginning of the two diffusion gradient pulses. Pilot studies showed that ADC values calculated from two b values were the same as ADC values calculated using regression analysis from four (0, 256, 558, and 1239) b values. The mean difference between these ADC values was only 0.93 ± 0.28% (n = 8). T2-weighted (80/2000/4), proton density–weighted, (20/2000/4), and T1-weighted (20/400/4) images were also obtained for the same section locations, section thickness, and field of view. Data from these scans were calculated as signal intensity ratios, that is, signal intensity in the ischemic brain divided by signal intensity from contralateral normal brain. Quantitative analysis of MR data was performed on one section centered at the optic chiasm (4 mm posterior to the rhinal fissure). This section was selected because it represented the location of maximal ischemia for the rat MCAO model used in the present study (18). Four regions of interest were analyzed: (*a*) basal ganglia in ischemic hemisphere; (*b*) basal ganglia in contralateral hemisphere; (*c*) cortex in ischemic hemisphere; and (*d*) cortex in contralateral hemisphere (Fig 1A).

Histologic Examination

After scanning on day 0, day 2, and day 6 after occlusion, brains were perfusion fixed with 200 mL of saline solution (0.9%) and 200 mL of paraformaldehyde (4%) in 0.1 M phosphate buffer from the left ventricle of the heart. Brains were postfixed in the same fixatives for 24 hours and placed in 20% glycerol and 2% dimethylsulfoxide in 0.1 M phosphate buffer for 48 hours, then were sectioned at 50 μm on a freezing microtome. Sections were incubated with 0.3% hydrogen peroxidase diluted with methanol for 30 minutes, followed by 10-minute washes in phosphate-buffered saline. For GFAP immunostaining, sections were incubated with 10% normal goat serum for 1 hour. Then these sections were incubated with primary antibody for GFAP (mouse antirat IgG, Boehringer Mannheim, Indianapolis, Ind) diluted with 2% normal goat serum

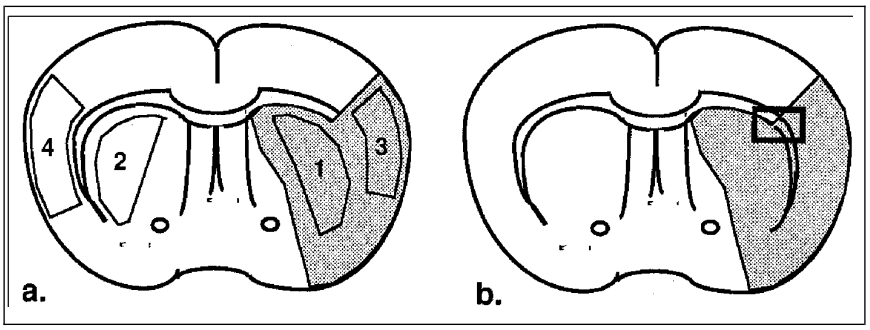

Fig 1. *a*, Regions of interest in the rat brain section used for quantitative MR analysis: *1*, basal ganglia in ischemic side, *2*, basal ganglia in contralateral side, *3*, cortex in ischemic side; and *4*, cortex in contralateral side. The *shaded area* represents the typical distribution of ischemia for this model.

b, Square region of interest indicates the area that is depicted in the histologic images (Fig 7). The area involves both ischemic basal ganglia and ischemic cortex.

and 0.5% sodium azide (1:200) overnight. After washing with phosphate-buffered saline, sections were placed in goat antimouse IgG conjugated with peroxidase (Boehringer Mannheim) diluted 1:300 in phosphate buffer and 2% goat serum for 3 hours. After washing with phosphate-buffered saline sections were developed by 3,3′-diaminobenzidine tetrahydrochloride and 0.03% hydrogenperoxidase in 50 mM Tris-hydrochloric acid buffer. For IgG immunostaining, sections were incubated with mouse antirat IgG antibody (Boehringer Mannheim) diluted 1:300 in phosphate buffer and 2% goat serum for 3 hours instead of incubation with first and second antibodies for GFAP staining. The sections were then developed with 3,3′-diaminobenzidine tetrochloride. Histologic examinations on the ischemic and contralateral hemisphere were also performed on the section centered at the optic chiasm (Fig 1B).

Statistical Analysis

For evaluation of temporal changes in each parameter, repeated-measures analysis of variance was used and then a Scheffe F test was applied to individual sets. For comparison between lesion and contralateral hemisphere or between basal ganglia and cortex for ADC and signal intensity ratio calculations, paired *t* tests were used. Correlations between various parameters were assessed with standard linear regression analysis. All data are expressed as mean ± SEM. Differences were considered to be significant at $P < .05$.

Results

Physiologic Variables

Systemic parameters were within normal limits (Table). Body temperatures were well controlled throughout the experiments including MR scanning on days 2 and 6 after MCAO.

MR Measurements

Diffusion-weighted scans on day 0 for all three groups showed increased signal intensity in the ischemic regions, primarily in the lateral basal ganglia and overlying cortex. Figure 2 shows changes in signal intensity ratio of diffusion-weighted images during early ischemic evolution (50 to 130 minutes after occlusion, group 1). Significant elevations in signal intensity ratio were present by 50 minutes after MCAO in basal ganglia ($P < .05$) and 70 minutes after MCAO in cortex ($P < .05$). Signal intensity ratio increased slightly over time and reached values of 1.43 (basal ganglia) and 1.28 (cortex) by 130 minutes after MCAO. Signal intensity ratios in basal ganglia were higher than those in cortex at every time point.

Measurements during the experiment

Time	Mean Arterial Blood Pressure, mm Hg	Body Temperature, °C	pH	$Paco_2$, mm Hg	Pao_2, mm Hg
Day 0 (n = 11)					
During surgery	86.27 ± 2.39	37.69 ± 0.21	7.39 ± 0.01	38.15 ± 1.83	126.59 ± 5.03
Before MR	101.75 ± 7.74	37.16 ± 0.29	7.34 ± 0.01	45.77 ± 1.46	153.40 ± 14.70
During MR	107.13 ± 4.90	37.29 ± 0.16			
After MR	100.34 ± 4.51	37.12 ± 0.16	7.32 ± 0.01	44.67 ± 2.28	148.22 ± 12.64
Day 2 (n = 8)					
During MR		37.70 ± 0.19			
Day 6 (n = 5)					
During MR		37.02 ± 0.32			

Note.—Values are mean ± SEM.

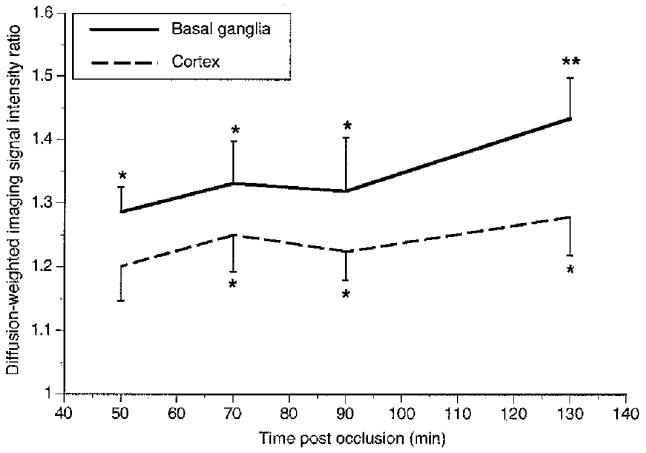

Fig 2. Temporal changes in signal intensity ratio of diffusion-weighted images from 50 to 130 minutes after MCAO. Data are shown as mean ± SEM.

* $P < .05$.

** $P < .01$ compared with contralateral side.

Diffusion-weighted images in the acute stage (2 hours after MCAO) showed high intensity in the ipsilateral hemisphere. After the early stage, signal intensities tended to decrease, returning to close to normal range during the intermediate stage (day 2). By day 6, diffusion-weighted scans showed well-demarcated regions of decreased intensity within the core of the ischemic lesion. A representative profile is shown in Figure 3. Quantitative analysis of the diffusion-weighted signal changes showed that by 2 hours after MCAO, ADC values were significantly lower than normal levels in the contralateral hemisphere ($P < .01$): 3.0 to 3.5 $\times$ 10^{-4} mm^2/s (ischemic) versus 5.7 to 5.9 $\times$ 10^{-4} mm^2/s (contralateral) (Fig 4). After this acute phase, ADC values in the ischemic brain began to increase; on day 2, ADC values in the ischemic lesion were indistinguishable from contralateral values; by day 6, ADC in ischemic brain became significantly increased compared with the contralateral side ($P < .05$), especially in basal ganglia (Fig 4).

A different temporal profile was present on conventional scans. Conventional MR images showed most significant changes on day 2. A typical temporal profile of T2-weighted scans is shown in Figure 3. In general, inconsistent changes were present on day 0, except for T2-weighted scans, in which signal intensity ratio was significantly increased in the basal ganglia ($P < .01$) (Fig 5). On T2-weighted scans, signal intensity was maximally increased by 30% to 60% above contralateral values on day 2. Changes on T1- and proton density–weighted scans were more modest (Fig 5). By day 6, some resolution of these signal changes had occurred, although on T2-weighted scans, signal intensity ratios were still significantly elevated (Fig 5).

From the acute to intermediate stage, increasing ADC values (Fig 4) seemed to track the evolution in T1- and T2-weighted signals (Fig 5), that is, the larger the subsequent change in T1- and T2-weighted signal intensity ratios on day 2, the more the ADC increased from day 0 to day 2. Linear regression analysis showed that increases in ADC values from day 0 to day 2 were significantly correlated with further changes of T1- and T2-weighted signal intensity ratios (Fig 6). However, there were no significant correlations between ADC change and changes in other MR parameters from intermediate (day 2) to late (day 6) stage: ADC change versus T1-weighted signal intensity ratio change ($r = .27$; $P = .45$), T2-

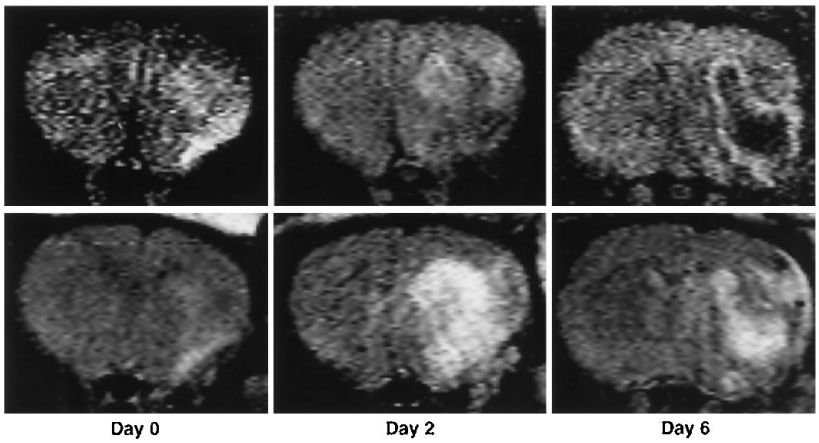

Fig 3. Temporal profiles of diffusion-weighted (*upper row*) and T2-weighted (*lower row*) imaging on day 0 (2 to 2.5 hours), day 2, and day 6 after MCAO.

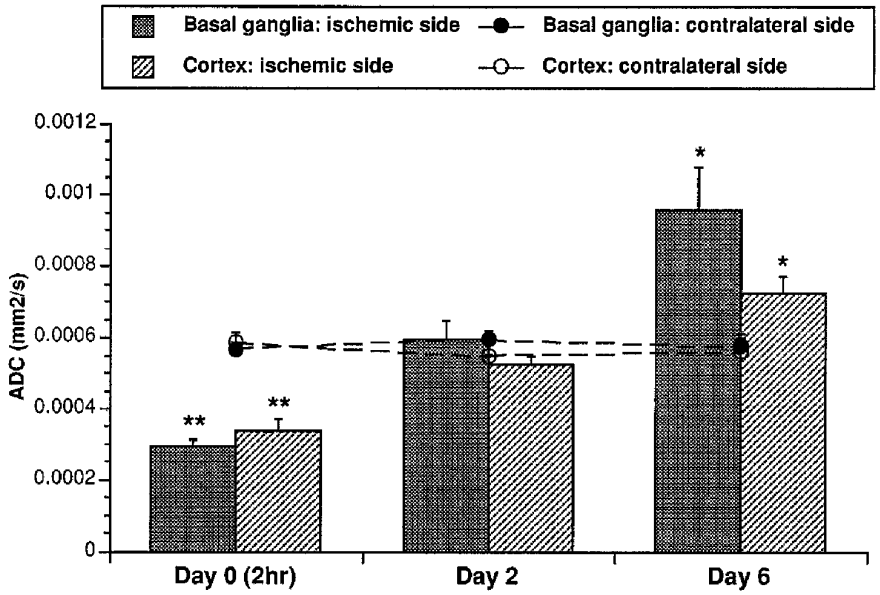

Fig 4. Temporal changes in apparent diffusion coefficients after MCAO in rats. Data are shown as mean ± SEM.
* $P < .05$.
** $P < .01$ compared with contralateral side.

weighted signal intensity ratio change (r = .04; P = .90) and proton density–weighted signal intensity ratio change (r = .05, P = .90).

Immunohistochemistry

Immunohistochemical results are shown in Figure 7. Cresyl violet staining showed that damage in basal ganglia tended to be more severe than that in cortex. At 4 hours after MCAO, the morphologic characteristics of early infarction (shrinkage and triangulation of cellular nuclei) were present in lateral basal ganglia. Although no extensive leakage of serum protein had occurred, there seemed to be some gathering of IgG within and around a few blood vessels in the ischemic areas. No increased GFAP staining was present. On day 2 after MCAO, clear infarction was present in lateral basal ganglia and ventral cortex. Reactive cells, presumably inflammatory cells and glial cells, were increased in number around the infarcted area. Intense IgG staining was seen extending from the ischemic core within the basal ganglia to the overlying cortex. GFAP staining showed intense gliotic activity around the border of the infarction. On day 6, the ischemic basal ganglia be-

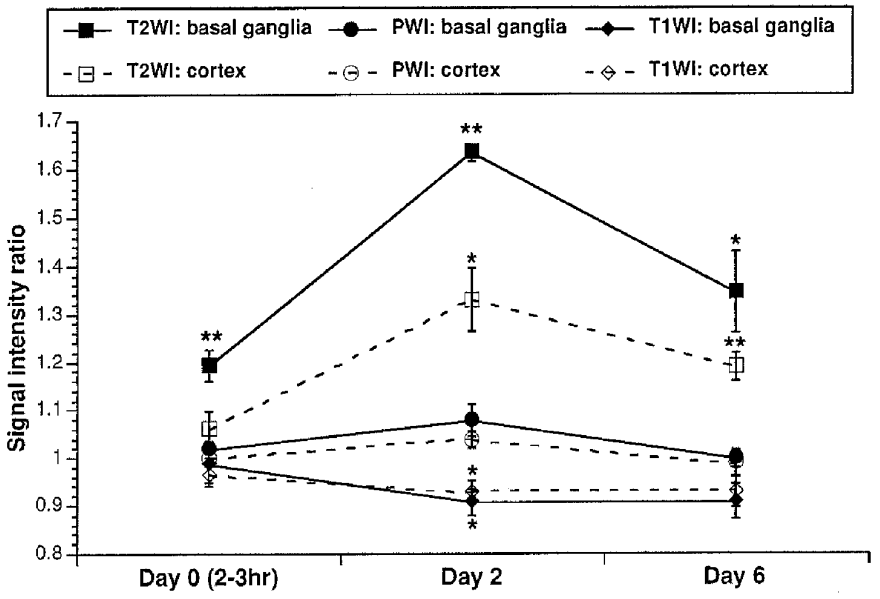

Fig 5. Temporal changes in signal intensity ratios of T2-weighted imaging (T2WI), proton density–weighted imaging (PWI), and T1-weighted imaging (T1WI) after MCAO in rats. Data are shown as mean ± SEM.
* $P < .05$.
** $P < .01$ compared with contralateral side.

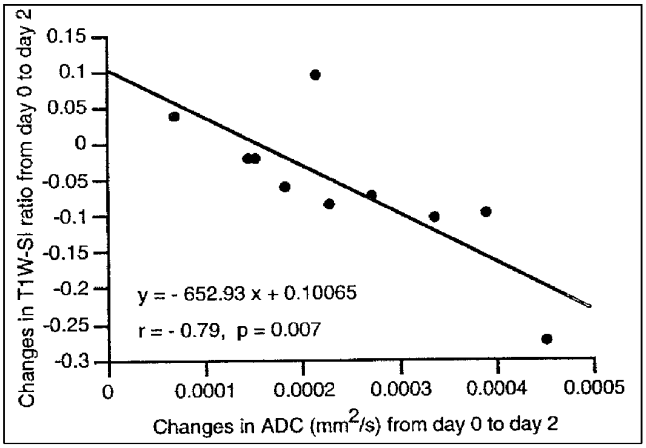

A

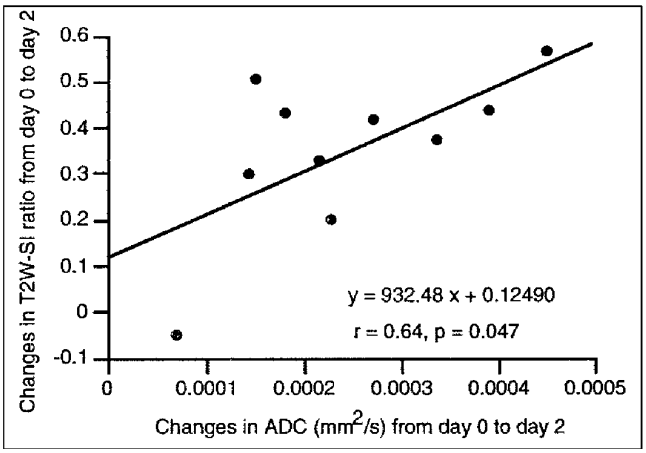

B

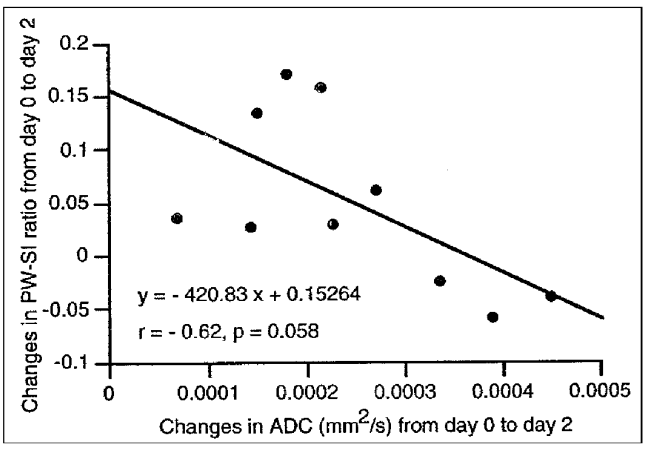

C

Fig 6. Correlations between changes in ADC from day 0 to day 2 and changes in signal intensity (SI) ratios of T1-weighted (T1W), T2-weighted (T2W), and proton density–weighted (PW) imaging from day 0 to day 2 after MCAO in the rat.

came totally necrotic and tended to be cystic with evidence of tissue cavitation. The adjacent cortex showed disruption of normal laminar structure as a result of neuronal degeneration. IgG-stained areas became widespread in the overlying cortex. GFAP staining slightly decreased around the border of the necrotic area but showed some spreading into the parietal cortex. Changes in the contralateral hemisphere in every staining were subtle compared with the ipsilateral hemisphere.

There was good correspondence between late (day 6) diffusion-weighted images and histologic damage; that is, core areas with tissue cavitation resulted in very high ADC values, whereas the hypercellular peripheral zone surrounding the cavitated core resulted in a boundary of low ADC values (Figs 7 and 8).

Discussion

Diffusion-weighted imaging allows the detection of acute ischemic brain injury as early as 30 minutes after onset, before lesions are seen on conventional spin-echo MR images (19). Diffusion-weighted imaging primarily reflects differences in the translational motion of water molecules (20, 21). The most likely explanation for the reduction of ADC in the early stages of ischemia is the migration of extracellular water into intracellular space as a result of reduced Na^+-K^+-adenosine triphosphatase activity (1–4). After this acute reduction in ADC, a complex process of ischemic evolution occurs, and ADC values tend to increase and recover toward normal levels (5–11). In the present study, we found that ADC values in ischemic brain were significantly reduced in the acute stage (2 to 3 hours), recovered back to normal range in the intermediate stage (day 2), and were significantly elevated by the late stage (day 6). In general, changes were more severe and rapid in the basal ganglia than in the cortex, reflecting the fact that the basal ganglia represents the ischemic core in this rat model of permanent focal ischemia.

Our results suggest that two distinct phases of ADC evolution occur after the initial acute stage of ischemia. In the first phase, a rapid renormalization of ADC values occurs over 48 hours after occlusion (from day 0 to day 2). ADC evolution from the acute to intermediate stage was quantitatively correlated with the development of signal intensity changes on con-

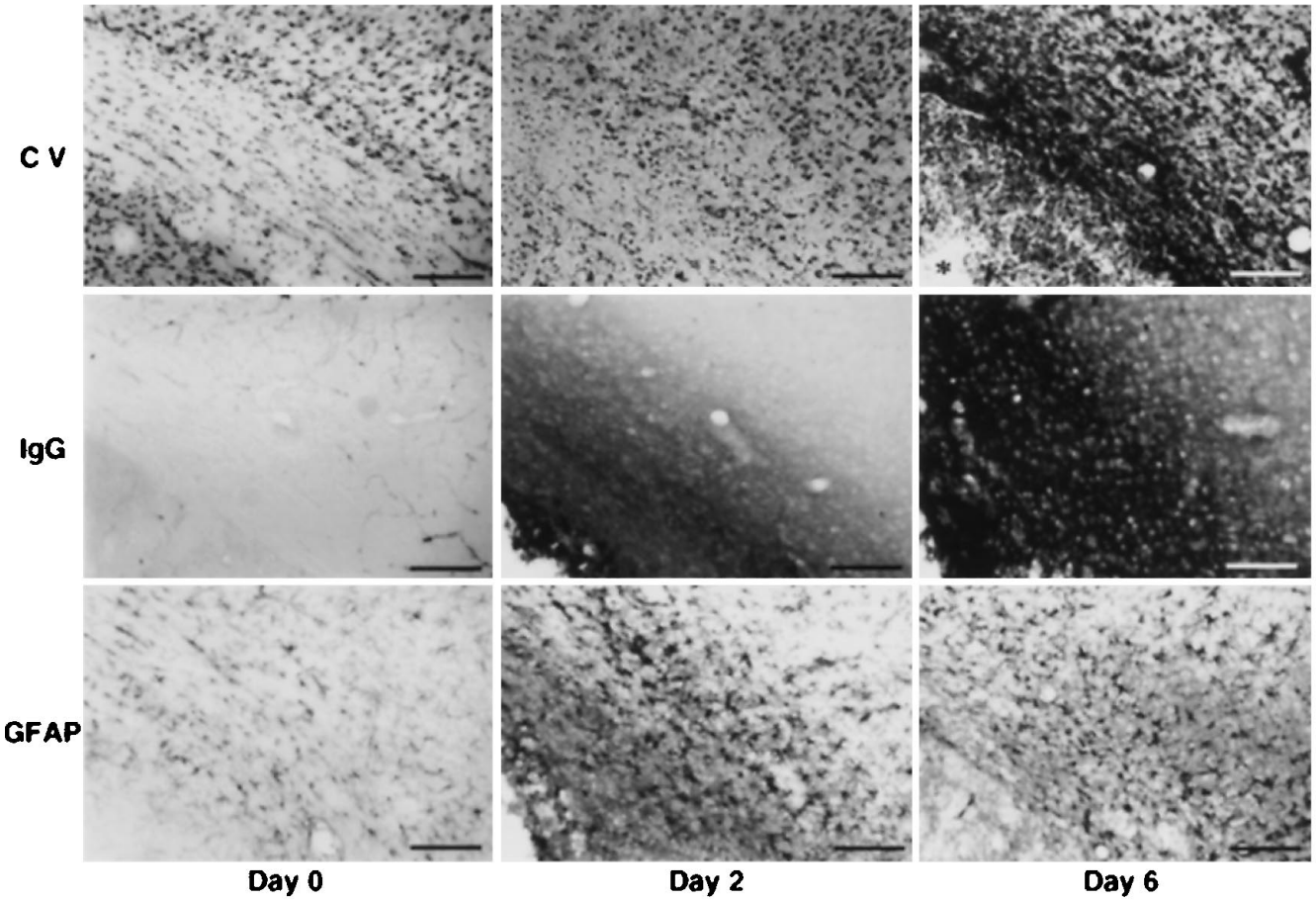

Fig 7. Immunohistochemical results on day 0, day 2, and day 6 after MCAO in the rat. Cresyl violet (*CV*) stainings (*upper row*) show subtle nuclear shrinkage in the basal ganglia on day 0, neuronal necrosis in the basal ganglia and the ventral cortex on day 2, and tissue cavitation (*asterisk*) with surrounding inflammatory cell infiltration on day 6. IgG stainings (*middle row*) show no remarkable leakage on day 0 and widespread leakage into the overlying cortex on days 2 and 6. GFAP stainings (*lower row*) show activated GFAP stainings in the cortex on days 2 and 6 compared with day 0. Each picture shows both ipsilateral cortex and basal ganglia and the lateral part of corpus callosum (see Fig 1B). *Bars* indicate 100 μm.

ventional spin-echo MR (T1- and T2-weighted images). It has been proposed that increased water content in the brain tissue after ischemia, which is caused by vasogenic edema, may greatly affect T1 and T2 relaxation times (22, 23). Our histologic data confirmed that, during this intermediate stage when maximal changes in signal intensity ratio were present on T2- and T1-weighted images, extensive infarction with leakage of serum proteins and GFAP activation was present. It has been shown using other models of experimental brain injury that serum

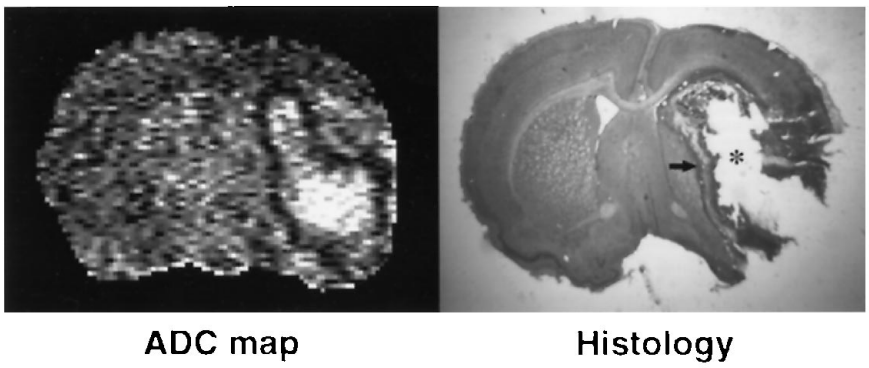

Fig 8. Comparison between ADC map and histologic image (cresyl violet staining) on day 6 after MCAO in rats. In the histologic section, the cystic core (*asterisk*), consisting of loose necrotic tissue with partial cavitation, corresponds with the area of increased ADC. The hypercellular peripheral zone (*arrow*) corresponds to a decreased ADC rim.

protein leakage and GFAP activation are markers of vasogenic edema (13–15). Therefore, the renormalization of ADC from the early to intermediate stage is most likely caused by the development of vasogenic edema. Increased tissue water content and higher extracellular volume fractions will result in higher diffusion coefficients (24). Other studies have shown that, for this rat model of ischemia, maximal elevations in brain tissue water content occur at 2 to 3 days after occlusion (25), which agrees well with the present results. In vasogenic edema, elevations in water content on the order of 3% to 4% can result in changes in ADC of 2.5 to 3.0 $\times$ 10^{-4} mm^2/s (22, 24). Additionally, parenchymal infarction during this intermediate stage may also lead to higher ADC values, because cell lysis will cause membrane fragmentation (10), dilution of proteins and cytoplasmic organelles into extracellular space, and ultimately loss of diffusive barriers (26).

The second phase of ADC evolution takes place over a longer period of time, from the intermediate (day 2) to the late (day 6) stage. This second phase is characterized by an elevation of ADC values above normal levels. However, there were no significant correlations between the further elevation of ADC values and the changes of T1- and T2-weighted signal intensity ratios. Histologic results in the late stage revealed widespread pannecrosis with cavitation in the core regions of the basal ganglia and selective neuronal degeneration in the overlying cortex. GFAP and IgG staining remained, demonstrating that gliotic activation and continued serum protein leakage via the damaged blood-brain barrier were still ongoing. These histologic findings can explain the significantly elevated ADC values in this stage. Cavitation is likely to increase ADC because of increased water mobility in the fluid-rich cystic regions. The hypercellular peripheral zone surrounding the cavitated core is visible as a rim of decreased ADC values. These results show that diffusion-weighted images can provide useful depictions of tissue characteristics (infarction, cavitation, and encapsulation) during the late stage of cerebral ischemia. Several other studies of stroke models have also shown increases of ADC as injury evolves from early to late stages (8, 12).

There are several limitations in the present study. First, we did not quantitatively correlate our MR data with histologic outcomes. It is very difficult to derive quantitative measures of ischemic severity from cellular histology. However, other studies have shown that semiquantitative grading of ischemic tissue injury is well correlated with ADC values (27). Second, although our results suggest that two phases of ADC evolution (acute-to-intermediate and intermediate-to-late) occur, we cannot provide quantitative data on precise rates of change in these MR parameters, because we did not map ADC evolution on a daily basis. The evolution of ADC changes may be highly nonlinear. Third, we could not obtain significant correlations between ADC evolution and proton density–weighted signal intensity ratio. This is probably because our proton density–weighted sequence used repetition times (2000 milliseconds) that were not long enough so that proton density–weighted signal were governed by both proton density and T1 relaxation (28). Finally, we did not measure cerebral blood flow in this study, so we were unable to obtain correlations between ADC alterations and the perfusion deficits present in our model.

In conclusion, the major findings of this study were: (*a*) after permanent focal ischemia in rats, a rapid renormalization of ADC occurs from the acute to intermediate stage that is highly correlated with the development of signal intensity changes on conventional spin-echo MR; (*b*) the renormalization of ADC is most likely caused by the development of vasogenic edema and cell lysis; and (*c*) further elevation of ADC values above normal during the late stage is related to the development of cavitation in severely infarcted tissue. Understanding these mechanisms of diffusion-weighted imaging changes can provide valuable pathophysiologic information on the course of ischemic stroke evolution. Determination of reversible and irreversible damage in the early stage and knowledge of intermediate and chronic outcomes in these corresponding regions will be crucial for clinical stroke treatment. It has already been shown that acute alterations in diffusion are reversible with reperfusion (29) or pharmacologic intervention (30). Further studies are now needed to follow noninvasively the effects of neuroprotective therapy over longer periods of time to see how early end points map onto later outcomes using quantitative MR techniques and analyses described in the present investigation.

Acknowledgments

We thank Tove Torgerson for assistance with the immunohistochemistry, Dr Elkan Halpern for valuable advice on statistical analysis, Dr Gilberto Gonzalez and Dr Gerald Wolf for their expert advice on MR protocols, and Dr Lee Schwamm for helpful discussions.

References

1. Moseley ME, Cohen J, Mintrovitch J, et al. Early detection of regional cerebral ischemia in cats: comparison of diffusion- and T2-weighted MRI and spectroscopy. *Magn Reson Med* 1990;14: 330–346
2. Moseley ME, Kucharczyk J, Mintorovitch J, et al. Diffusion-weighted MR imaging of acute stroke: correlation with T2-weighted and magnetic susceptibility-enhanced MR imaging in cats. *AJNR Am J Neuroradiol* 1990;11:423–429
3. Benveniste H, Hedlund LW, Johnson GA. Mechanism of detection of acute cerebral ischemia in rats by diffusion-weighted magnetic resonance microscopy. *Stroke* 1992;23:746–754
4. Mintrovitch J, Yang GY, Shimizu H, Kucharczyk J, Chan PK, Weinstein PR. Diffusion-weighted magnetic resonance imaging of acute focal cerebral ischemia: comparison of signal intensity with changes in brain water and Na^+,K^+-ATPase activity. *J Cereb Blood Flow Metab* 1994;14:332–336
5. Knight RA, Ordidge RJ, Helpern JA, Chopp M, Rodolosi LC, Peck D. Temporal evolution of ischemic damage in rat brain measured by proton nuclear magnetic resonance imaging. *Stroke* 1991;22: 802–808
6. Chien D, Kwong KK, Gress DR, Buonanno FS, Buxton RB, Rosen BR. MR diffusion imaging of cerebral infarction in humans. *AJNR Am J Neuroradiol* 1992;13:1097–1102
7. Warach S, Chien D, Li W, Ronthal M, Edelman RR. Fast magnetic resonance diffusion-weighted imaging of acute human stroke. *Neurology* 1992;42:1717–1723
8. Verheul HB, Berkelbach van der Sprenkel JW, Tulleken CA, Tamminga KS, Nicolay K. Temporal evolution of focal cerebral ischemia in the rat assessed by T2-weighted and diffusion-weighted magnetic resonance imaging. *Brain Topogr* 1992;5:171–176
9. Helpern JA, Dereski MO, Knight RA, Ordidge RJ, Chopp M, Qing ZX. Histopathological correlations of nuclear magnetic resonance imaging parameters in experimental cerebral ischemia. *Magn Reson Imaging* 1993;11:241–246
10. Pierpaoli C, Righini A, Linfante I, Tao-cheng JH, Alger JR, Di Chiro G. Histopathological correlates of abnormal water diffusion in cerebral ischemia: diffusion-weighted MR imaging and light and electron microscopy study. *Radiology* 1993;189:439–448
11. Knight RA, Dreski MO, Helpern JA, et al. Magnetic resonance imaging assessment of evolving focal cerebral ischemia. *Stroke* 1994;25:1252–1262
12. Takahashi M, Fritz-Zieroth B, Chikugo T, Ogawa H. Differentiation of chronic lesions after stroke in stroke-prone spontaneously hypertensive rats using diffusion-weighted MRI. *Magn Reson Med* 1993;30:485–488
13. Schmidt-Kastner R, Szymas J, Hossmann KA. Immunohistochemical study of glial reaction and serum-protein extravasation in relation to neuronal damage in rat hippocampus after ischemia. *Neuroscience* 1990;38:527–540
14. Amaducci L, Forno KI, Eng LF. Glial fibrillary acidic protein in cryogenic lesion of the rat brain. *Neurosci Lett* 1981;21:27–32
15. Sundstrom R, Kalimo H. Extracellular edema and glial response to it in the cerebellum of suckling rats with low-dose lead encephalopathy. *Acta Neuropathol* 1987;75:116–122
16. Tamura A, Graham DI, McCulloch J, Teasdale GM. Focal cerebral ischemia in the rat, I: description of technique and early neuropathological consequences following middle cerebral artery occlusion. *J Cereb Blood Flow Metab* 1981;1:53–60
17. Bederson JB, Pitts LH, Tsuji M, Nishimura MC, Davis RL, Bartkowski H. Rat middle cerebral artery occlusion: evaluation of the model and development of a neurologic examination. *Stroke* 1986;17:472–476
18. Duverger D, MacKenzie ET. The quantification of cerebral infarction following focal ischemia in the rat: influence of strain, arterial pressure, blood glucose concentration, and age. *J Cereb Blood Flow Metab* 1988;8:449–464
19. Mintorovitch J, Moseley ME, Chileutt L, Shimizu H, Cohen Y, Weinstein PR. Comparison of diffusion- and T2-weighted MRI for the early detection of cerebral ischemia and reperfusion in rats. *Magn Reson Med* 1991;18:39–50
20. Stejskal EO, Tanner JE. Spin diffusion measurements: spin echos in the presence of a time-dependent field gradient. *J Chem Physics* 1965;42:288–292
21. Le Bihan DL, Breton E, Lallemand D, Aubin ML, Vignaud J, Laval-Jeantet M. Separation of diffusion and perfusion in intravoxel incoherent motion MR imaging. *Radiology* 1988;168:497–505
22. Naruse S, Horikawa Y, Tanaka C, Hirakawa K, Nishikawa H, Yoshizaki K. Proton nuclear magnetic resonance studies on brain edema. *J Neurosurg* 1982;56:747–752
23. Horikawa Y, Naruse S, Tanaka C, Hirakawa K, Nishikawa H. Proton NMR relaxation times in ischemic brain edema. *Stroke* 1986;17:1149–1152
24. Ebisu T, Naruse S, Horikawa Y, et al. Discrimination of different types of white matter brain edema using magnetic resonance diffusion weighted imaging. *J Magn Reson Imaging* 1993;3:863–868
25. Goto O, Asano T, Koide T, Takakura K. Ischemic brain edema following occlusion of the middle cerebral artery in the rat, I: the time course of the brain water, sodium and potassium contents and blood-brain barrier permeability to ^{125}I-albumin. *Stroke* 1985; 16:101–109
26. Garrido L, Wedeen VJ, Kwong KK, Spencer UM, Kantor HL. Anisotropy of water diffusion in the myocardium of the rat. *Circ Res* 1994;74:789–793
27. Jiang Q, Zhang ZG, Chopp M, et al. Temporal evolution and spatial distribution of the diffusion constant of water in rat brain after transient middle cerebral artery occlusion. *J Neurol Sci* 1993;120:123–130
28. Hendrick RE. Image contrast to noise. In: Stark DD, Bradley WG Jr, eds. *Magnetic Resonance Imaging*. St Louis: CV Mosby, 1988: 66–83
29. Minematsu K, Li L, Sotak CH, Davis MA, Fisher M. Reversible focal ischemic injury demonstrated by diffusion-weighted magnetic resonance imaging in rats. *Stroke* 1992;23:1304–1311
30. Lo EH, Matsumoto K, Pierce A, Garrido L, Luttinger D. Pharmacologic reversal of acute changes in diffusion-weighted magnetic resonance imaging in focal cerebral ischemia. *J Cereb Blood Flow Metab* 1994;14:597–603